Original Article

Comparing and evaluating the efficacy of the TOR18FG Leeds test X-ray phantom for T-rays

Elise Maree Pogson[1,2], Joanne McNamara[3], Peter Metcalfe[2], Roger A Lewis[1]

[1]Institute for Superconducting and Electronic Materials, University of Wollongong, Wollongong, NSW 2522, Australia; [2]Centre for Medical Radiation Physics, University of Wollongong, Wollongong, NSW 2522, Australia; [3]Department of Medical Physics, Illawarra Cancer Care Centre, Locked Bag 8808, South Coast Mail Centre, Wollongong, NSW 2521, Australia

Corresponding to: Elise Maree Pogson. Centre for Medical Radiation Physics, University of Wollongong, Wollongong, NSW 2522, Australia. Email: emp993@uowmail.edu.au.

Abstract: The commercially available X-ray fluoroscopy quality assurance phantom, the Leeds test object TOR18FG, was found to be suitable to assess T-ray image quality in the range (0.1-0.4) THz at a depth of 0.5 cm. Previous to this only custom made phantoms, made especially for the T-ray region, assessed T-ray spatial resolution. However, if sub-wavelength techniques are used, the Leeds test phantom may be implemented to measure the T-ray systems spatial resolution, allowing us to directly compare X-ray and T-ray spatial resolution. The systems compared include a Gulmay Orthovoltage machine (X-ray), the On Board Imager (OBI) of a Varian linear accelerator (X-ray), a two-colour system (T-ray) and Terahertz Time Domain Spectroscopy (THz-TDS) system. X-rays were found to have a spatial resolution of 1.25 lp/mm using the On Board Imager of a Varian Linear Accelerator whilst T-rays imaged using a broadband source imaged through a spatial pinhole had a spatial resolution of 0.56 lp/mm. The TOR18FG background material was found to block, 90% and 99% of the broadband T-rays emitted from a THz-TDS photo-conductive emitter, at 0.4 THz and 0.53 THz respectively. Contrast sensitivity was found to be 3% for 25 cm × 25 cm X-ray field at 65 kV, whilst this value could not be established for T-rays using the TOR18FG. All contrast circles were found to be the same for T-rays i.e. all 40% at 0.1 THz. Images of the same leaf were taken with diagnostic X-rays and both broadband and continuous wave (CW) T-ray systems. T-rays proved superior in providing image contrast, for a hydrated leaf, over X-rays.

Key Words: Terahertz; X-ray; imaging; resolution

Submitted Jan 27, 2013. Accepted for publication Feb 27, 2013.
doi: 10.3978/j.issn.2223-4292.2013.02.05
Scan to your mobile device or view this article at: http://www.amepc.org/qims/article/view/1588/2206

Introduction

Terahertz radiation, also known as T-rays or THz (1 THz = 1×10^{12} Hz), refers to the region of the electromagnetic spectrum between 100 GHz and 30 THz (wavelengths of approximately 3 mm to about 1 μm) (1). Until recently the T-ray region (also known as the "Terahertz Gap") has been a relatively difficult area of the electromagnetic spectrum when it comes to reliability, expense and product development. This is because sources and detectors were bulky, expensive or required cooling (such as a liquid helium cooled bolometer). Current sources and detectors can operate at room temperature opening up this wavelength range to many new possibilities and applications. These possible applications include: biomedical imaging (2,3), detection of structural defects (4), drugs testing (5), defence and security applications (6), art analysis/reconstruction (7) and medical imaging. Examples of medical imaging applications include: wound healing (8,9), detection of carcinomas (10) and breast cancer's tumour margin definition and detection (11-13).

There have been many review articles (1,12-15) stating the potential for T-ray imaging. Theoretically, T-rays have some advantages over X-rays (14). T-rays are less harmful

to biological tissue and have lower Rayleigh scattering when compared to X-rays. T-rays have low photon energies (for example, 4 meV at 1 THz) and are therefore non-ionising. Many proposed T-ray imaging applications exploit the unique capabilities of T-ray radiation to penetrate common packaging materials and provide spectroscopic information about the materials within (15). Imaging through packaging using T-rays has been demonstrated many times, e.g., chocolate being imaged behind its wrapping using an X-Y stage (16). Current imaging techniques include imaging using broadband raster scanning, the time domain approach, time of flight imaging (17), 3D tomography (18), video-rate imaging (19), single shot imaging (20), and CW imaging. Techniques have also been developed that image below the diffraction limit to provide better resolution. These include near-field imaging (21), near-field optical microscopy (22), and emission imaging (15).

X-ray and T-ray imaging are vying to be used for shared purposes such as security screening, material quality assurance and medical imaging. X-rays are a developed technology with good resolution, providing sharp images for materials with high atomic numbers provide greater image contrast for example metal scissors, bone and circuits. T-rays are shown to be more effective at imaging materials with lower atomic numbers these are materials for which diagnostic X-rays provide low or no contrast. Both X-rays and T-rays can image through packing material, however T-rays can provide a spectral fingerprint in which materials of interest such as explosives, biological material or drugs may be identified.

Image quality is assessable using terms such as contrast, resolution and artifacts. There are no discernible artifacts in the images presented in this paper. Here contrast and resolution are assessed using the TOR18FG Leeds test phantom. Spatial resolution is the size in the imaging plane of the smallest resolvable object. Sub-wavelength techniques withstanding, this corresponds to the radius of the smallest spot to which a collimated beam of light may be focused. This is proportional to the wavelength used. To measure how closely lines can be resolved in an image a test pattern is implemented, the pattern resolved with the smallest gap between lines is the measure of the systems spatial resolution in line pairs per mm (lp/mm). This method has been shown previously for Terahertz Pulsed Imaging (TPI) (23) using specially designed phantoms for the T-ray range. The spatial resolution was limited to the T-ray wavelength (beam waist) as expected. Other custom built phantoms include: a contrast nylon step wedge phantom (23), a point spread function phantom for reflection imaging (24), Teflon substrate printed circuit boards (25), test pattern printed using lithographic techniques at various depths for 3D spatial resolution evaluation (26) and Silicon plates with gratings stacked (27). This paper is measuring the spatial resolution at a depth of 0.5 cm inside a 1 cm phantom. An ideal back-ground material for a phantom would be highly transmissive with a low absorption coefficient. Alternatively a thin phantom would be ideal. A 1 cm phantom may be acceptable if the absorption coefficient is extremely low, such as for Polystyrene. Similarly to 3D imaging (26), the THz signal will penetrate through layers of different materials and encounters beam diffusion, material dispersion, angle-dependent multiple reflection and transmission, and other interactions within the medium, which will ultimately affect the spatial resolution. Contrast is the difference in luminance that makes an object distinguishable. Contrast can be assessed using the Michelson contrast formula [1], where I is the intensity.

$$\text{Contrast}(\%) = 100 \times \left(\frac{I_{max} - I_{min}}{I_{max} + I_{min}} \right) \quad [1]$$

This article aims to directly compare X-ray and T-ray image quality and assess a commercially available test pattern capable of measuring this using both systems.

Materials and methods

The resolution of T-ray and X-ray systems is established using the same Leeds test pattern. From this a direct comparison is made. The Leeds fluoroscopy test phantom has resolution test patterns of 0.5 to 5 lp/mm. This test pattern is typically purchased for routine quality control procedures for diagnostic radiology. This TOR18FG model is specifically used in fluoroscopy and fluorography on a regular basis (weekly/monthly) (28). This phantom allows measurement of image quality by monitoring brightness and contrast levels, determining the resolution limit, and by finding the low-contrast sensitivity. There are 18 details/circles of 8 mm diameter with a contrast range of 0.009 to 0.167 at 70 kV using 1 mm of Copper on top (28). Test objects have been manufactured at Leeds University since 1955 on an in house basis; since 1979 fluoroscopy test objects have become available commercially (29).

T-ray equipment

Two sources have been used; one generating CW T-rays,

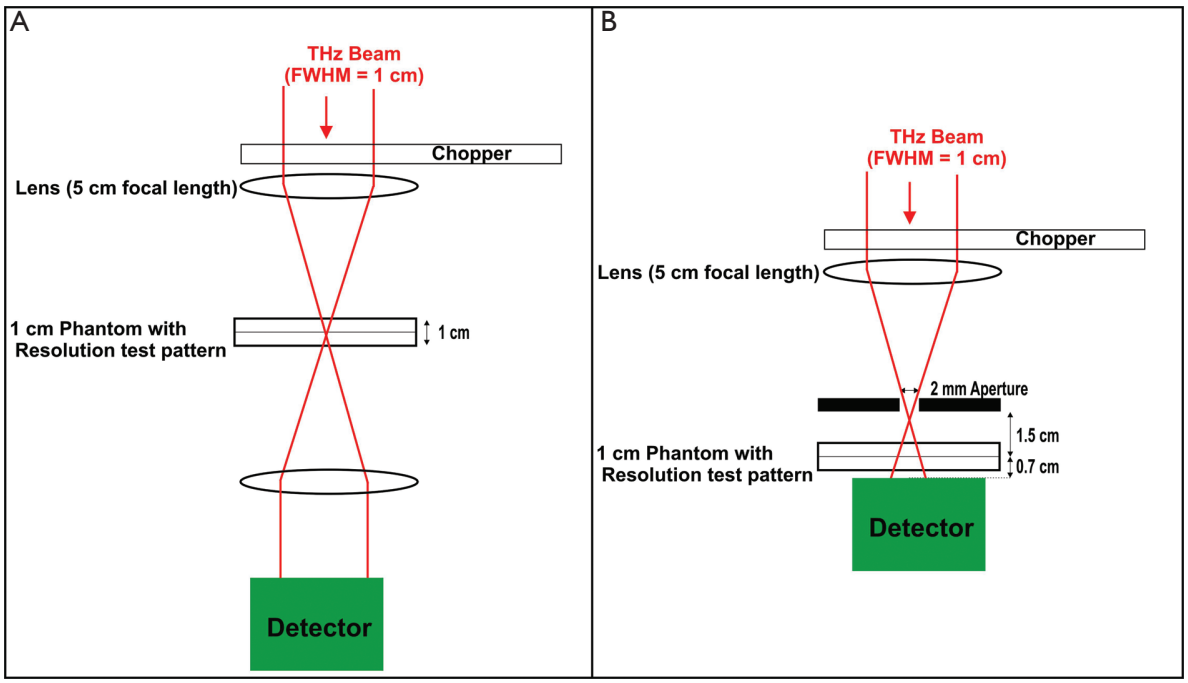

Figure 1 Set-up for T-ray imaging, not to scale with (A) normal detection method and (B) Sub-wavelength detection

and the other broadband T-rays. To generate broadband T-rays an emitter is pumped by laser operating with 350 mW producing a 790 nm beam to produce T-rays. This signal is higher at some frequencies than others, and falls off before 0.1 THz and after 1 THz to under −10 dB (measured with an electro-optic detector as in spectroscopy measurements). Thus its frequency range will be referred to as 0.1-1 THz. This is the same as in THz-TDS systems, outlined previously (30), however here the signal has been diverted to an imaging stage and detector as shown in *Figure 1A,B*, rather than being incident upon a sample and an electro-optic detector as in spectroscopy.

Each image has the signal taken at each point using an X-Y stage after chopping at 1 kHz for both the broadband and CW sources. Two room temperature detectors, a Golay Cell and a Schottky detector, have been used. The two-colour system set-up using the Golay Cell is a CW system with a tunable range of 0.06-1 THz. In this case the physical chopper which modulates the input is replaced by biasing the emitter with a 13.5 Hz sine wave signal of amplitude ±8 V to decrease background thermal radiation apparent when using a chopper. If the Schottky detector is in use, the emitter is biased by a 1 kHz sine wave and allows for faster scanning times. Even faster times are possible using the two-colour system if this modulation frequency is increased, and can be increased up to 25 kHz (31). Further details of the T-ray imaging systems can be found in *Figure 1*. The two-colour system is outlined in *Figure 2*. Here the detector may again be changed to the Golay Cell or the Schottky detector. It should be noted that different detectors have different responses i.e. the Schottky detector has a better response for lower frequencies than the Golay Cell. The Golay Cell is the detection method used on the two-colour system which generated the images in *Figure 3B,E*. The Golay detector was also used in conjunction with the photo-conductive emitter from the THz-TDS system to generate *Figure 3C,F*.

THz-TDS has formerly been implemented for spectroscopy as outlined previously (30) using electro-optic balanced detectors rather than Schottky or Golay broadband detectors. Spectroscopy has also been performed here to determine the wavelengths able to penetrate the Leeds test phantom. The procedure for this has also been outlined previously (30).

X-ray equipment

There are two X-ray sources applied here to generate different kV X-rays. The first is that of a Varian linear accelerator On-Board Imager (OBI) (Varian Medical Systems, Inc. Palo Alto, CA) with a 150 kV X-ray tube source and an amorphous silicon flat-panel X-ray image

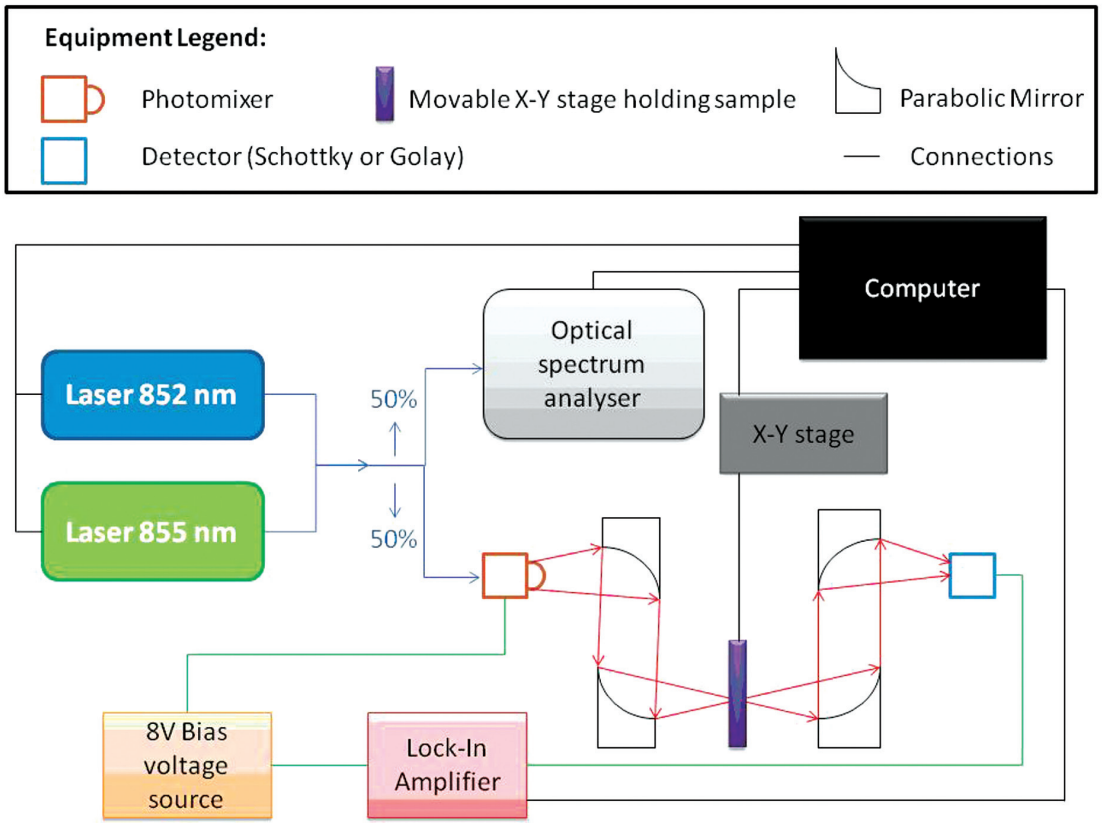

Figure 2 Experimental two-colour imaging system

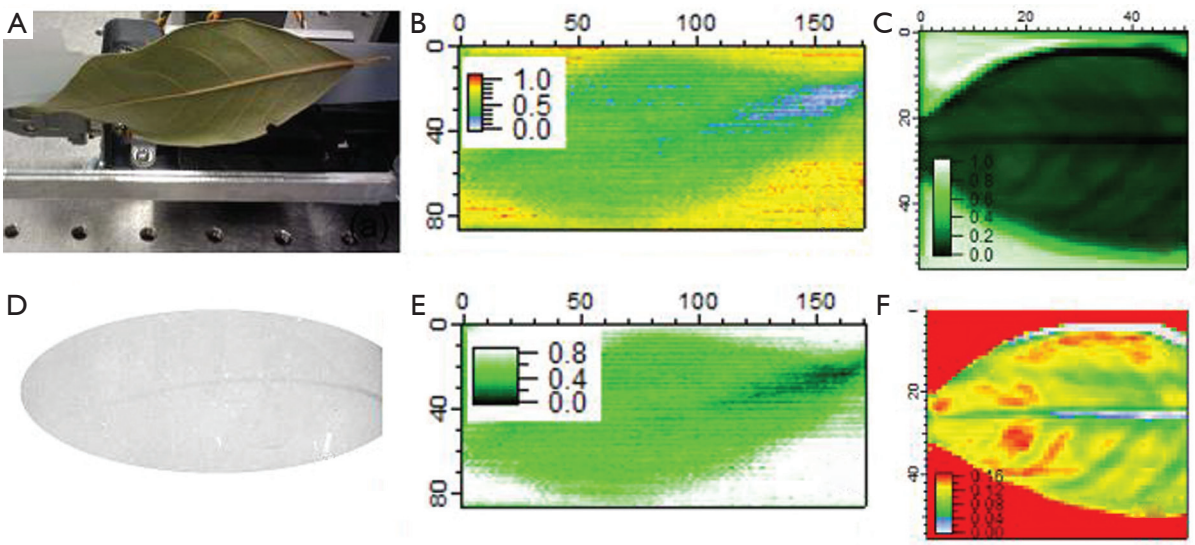

Figure 3 Hydrated leaf imaged using (A) visible camera (B) T-rays on the two-colour system (0.45 THz), (C) the broadband source, (D) X-rays on Orthovoltage unit at 50 kV, (E) T-rays on the two-colour system with transmittance scaled to 0.8 for clarity and (F) the broadband source scaled to 0.16 transmittance for clarity

Table 1 T-ray and X-ray systems

Equipment	X-ray OBI	X-ray orthovoltage	T-ray two-colour system	T-ray THz-TDS
Output	X-rays (50-150 kV)	X-rays (50-250 kV)	0.06-1 THz CW	0.1-1 THz Broadband
Power	3.75 kW at 75 kV	1 kW at 50 kV	10 μW at 1THz	Few nW with peak powers of order 10^1 μW
Detector	Varian Flat-bed Panel	EBT Gafchromic Film	Golay Cell, Schottky	Golay Cell, Schottky

detector. The second, providing lower energies, is from a Gulmay D3300 (Gulmay Ltd, Chertsey, UK) X-ray unit set to a tube voltage of 50 kV using GAFCHROMIC EBT film (International Specialty Products, Wayne, NJ) as a detection method. The films are then scanned and thus transformed into a digital image. OBI is in practise for image guided radiotherapy and Gulmay Orthovoltage units usually for palliation and skin treatment (32). Whilst Orthovoltage machines are typically used for producing higher energy X-rays than OBI, we have exploited the ability of the Gulmay unit (Kilovoltage and Orthovoltage source) to produce superficial X-rays here due to this unit's large range (refer to *Table 1*). It has been set at 50 kV with film as the resolution is better than OBI and may provide object outlines where the OBI does not. Overviews of each system as used here are given in *Table 1*.

Results and discussion

Images

X-rays have a limiting spatial resolution of approximately 50 μm due to Rayleigh scattering (33). Spatial resolution is also limited by the detector (34). T-rays will generally be expected to have lower resolution, as the detection method outlined here for the T-rays relies on an X-Y stage to raster scan the image and the resolution is limited by the wavelength (e.g., 0.3 mm at 1 THz) using normal imaging techniques as in *Figure 1A*. However if sub-wavelength techniques such as introducing a pinhole or aperture (35) (*Figure 1B*) or near field detection (36) or open aperture method used [THz wave is focused into a tapered metal-tip aperture and the sample is scanned in the near field (37)] are implemented the resolution and contrast is enhanced (27). Apertureless THz-scanning near-field optical microscopy (THz-SNOM) has recently been demonstrated in the THz region, where the resolving aperture is substituted by a sharp tip and the scattering of the incident wave is measured and has been found to have spatial resolution as small as 40 nm (λ/3,000) (36,38). T-ray image resolution may also be improved by setting the CW system to generate shorter wavelengths, due to their tighter beam waist. Other detection methods may also improve this such as an array or source array and detector (39).

One example of where T-ray imaging provides better contrast and image quality than X-ray imaging is shown in *Figure 3*. The leaf was not detected at all using the OBI and was barely detected using X-rays from the Gulmay Orthovoltage/Kilovoltage source set at 50 kV. This is shown in *Figure 3D*.

However using T-ray broadband sources the freshly cut (within 2 hours) leaf, its veins and hydration is clearly shown in *Figure 3C,F*. This has been shown in more detail previously and with better resolution (40,41), here we aim to compare both Terahertz systems without sub wavelength techniques with X-rays. The leaf is imaged using the broadband source (THz-TDS photoconductive emitter) as set-up in *Figure 1A*. The CW imaging performed on the two-colour system at 0.45 THz also displays the leaf but not as well as the 0.1-1 THz broadband source. Both are imaged with the Golay Cell as the detector, set-up as in *Figure 1A*. The resolution of the X-ray image is better (scanner set to 258×146 pixels and OBI with 1,024×768 pixels) than those obtained using the T-ray broadband (55×50 pixels, *Figure 3C,F*) and CW (170×86 pixels, *Figure 3B,E*) systems. Despite this T-ray images show the hydration clearer than X-rays.

Resolution determined using the Leeds test phantom

Using standard wavelength T-ray imaging as shown in *Figure 2* and *Figure 1A*, the resolution test pattern was unable to be distinguished as shown in *Figure 4*. The spatial resolution of both T-ray system's when set-up, as shown in *Figure 1A* and *Figure 2*, are both limited to their wavelength λ. For example, at a T-ray frequency of 0.1 THz the wavelength is 3 mm giving a spatial resolution of 3 lp/mm. This is ensured by the step sizes of the x-y stage always having a smaller value than the wavelength limit. The broadband source 0.1-1 THz and CW source 0.06-1 THz

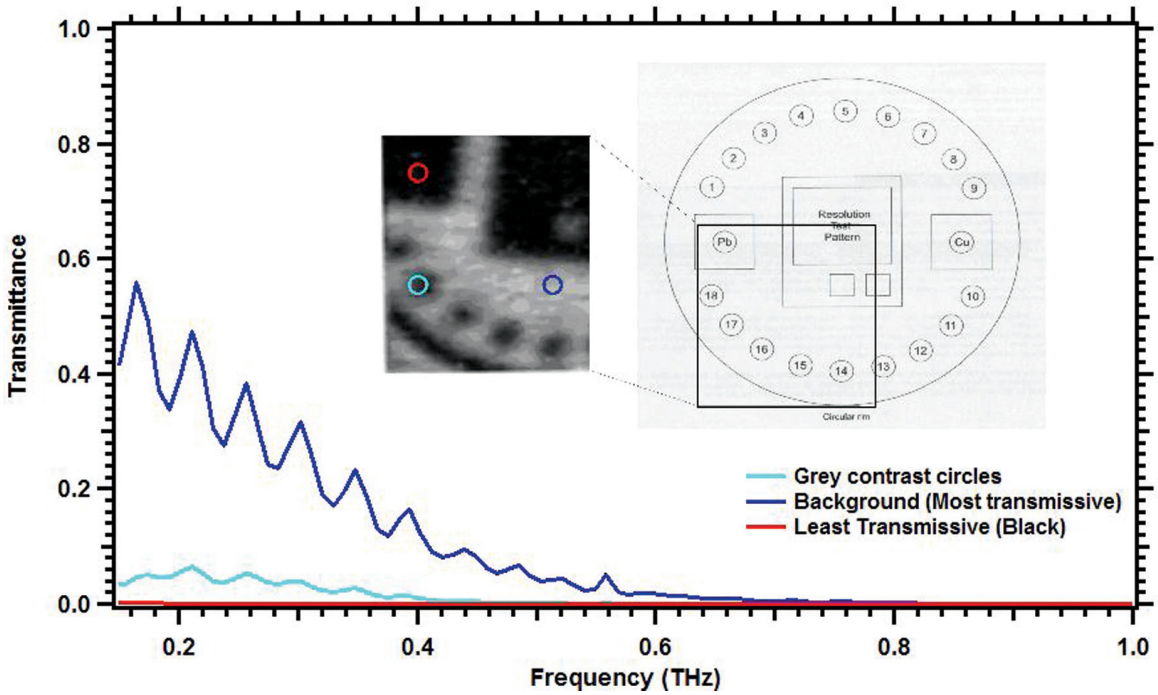

Figure 4 T-ray transmittance through Leeds test phantom. Inset are the regions measured [image is from CW source at 0.1 THz, and outline from booklet (42)]

were both not able to image the phantom's resolution test pattern using both Schottky and Golay detectors when set up as in *Figure 1A*.

However, shorter wavelengths (higher frequencies of approximately 0.8 THz and larger) should have a beam waist capable of determining the 0.5 lp/mm test pattern. Unfortunately these may not be penetrating the test phantom. Spectroscopy was performed on the Leeds test phantom to determine the frequencies penetrating the test phantom. The transmittance results are shown in *Figure 4*.

The test pattern lines are expected to be as transmissive as the background region of the Leeds test phantom. It may be seen that higher frequencies are not penetrating the phantom. Sub-wavelength techniques are necessary for the penetrating frequencies 0.1-0.4 THz to resolve the Leeds test pattern. Thus an aperture was placed in front of the broadband source as shown in *Figure 1B*. This confocal microscopy technique can enhance the lateral resolution of the system up to $\lambda/4$ (36). The Leeds test phantom was then able to be resolved as shown in *Figure 5A*.

The spatial resolution of the broadband T-rays is 0.56 lp/mm, as shown in *Figure 5*. This is what you would expect from an aperture, as theoretically the spatial resolution will reduce to the size of the aperture used (36). The cut-off frequency for the dominant transverse electric mode (TE_{11}) is given by $f_{cut\text{-}off}=1.8412\times c/r$ to be 0.088 THz [where r is the radius of 1 mm, and c is the speed of light (m/s) and thus would not screen out the majority of the THz signal (0.088-0.4 THz)] (36). Without sub-wavelength techniques X-rays will always have a higher spatial resolution due to their smaller wavelengths.

The X-ray spatial resolution is 1.25 line pair mm^{-1} measured using the TOR18FG Leeds test phantom for a 25 cm × 25 cm field size. This is a resolution limit of 0.8 mm giving a better resolution than the confocal microscopy broadband T-rays with resolution limit of 1.79 mm (0.56 lp/mm).

T-ray specifically designed bar patterns have previously been measured using T-ray Pulsed Imaging (TPI) systems (23) that showed 0.5 THz and 1 THz to have limiting spatial frequencies of 0.7 and 1.2 line pair mm^{-1} respectively (where the Modulation Transfer Frequency was 20%) which are ~λ. This is similar to our measurement of broadband (0.1-0.4) THz having spatial resolution of 0.56 lp/mm using the confocal microscopy technique. The Leeds test phantom has the advantage of being able to be applied for both X-ray and T-ray systems. However the T-ray systems must be either: of low frequency and higher power than typical THz-TDS systems or using

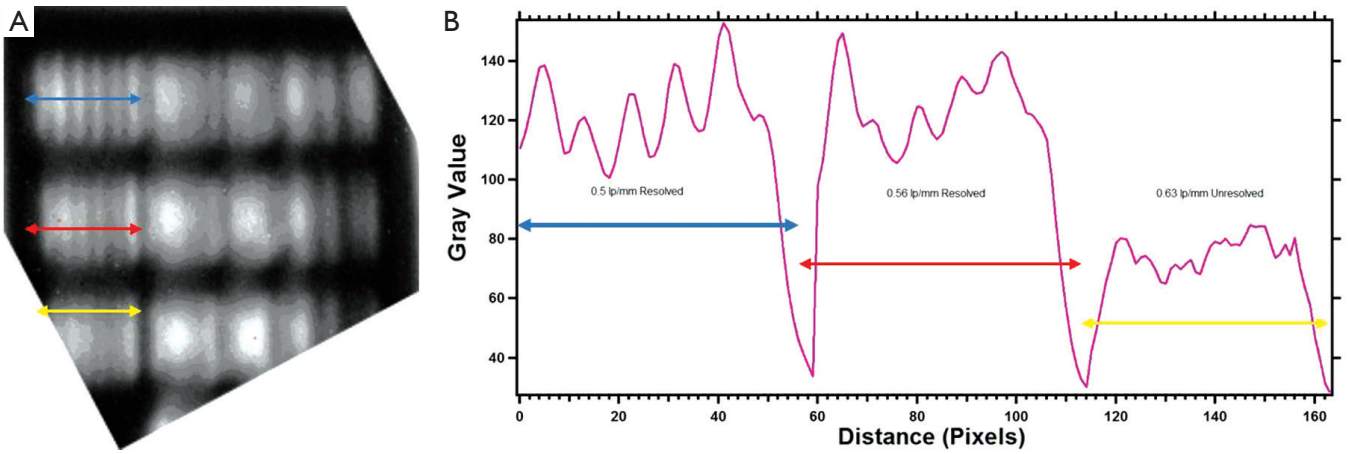

Figure 5 Leeds test phantom (A) T-ray Broadband Image and (B) T-ray line pair profiles

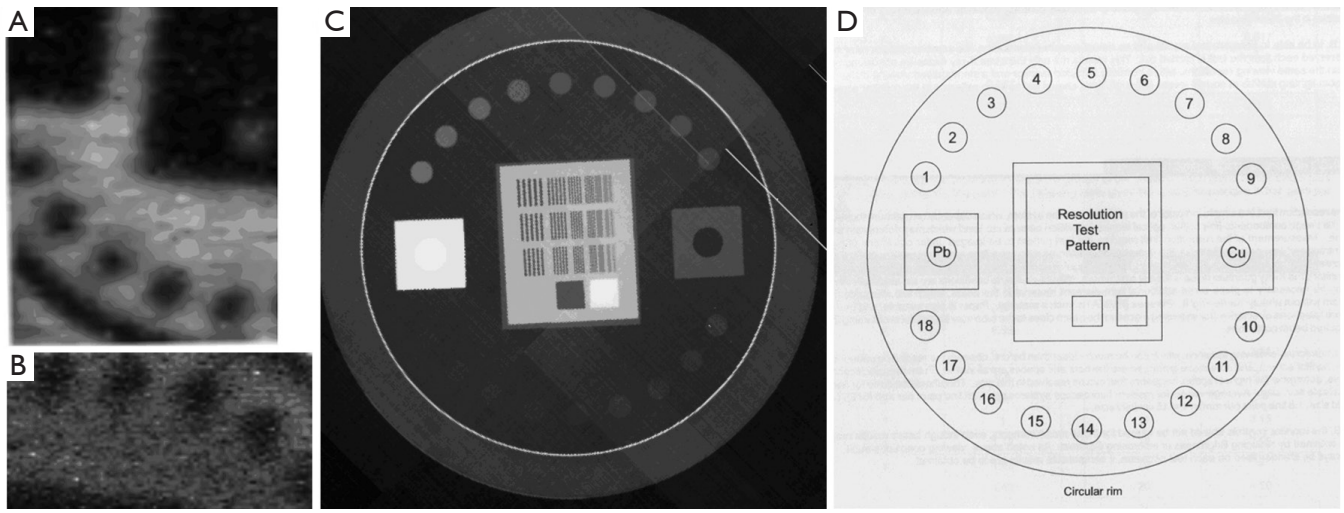

Figure 6 The Leeds test phantom contrast images using (A) 0.1 THz showing circles 14-18, (B) 0.3 THz showing circles 4-7, (C) 65 kV X-rays showing circles 1-13, and (D) Leeds booklet outline (42)

subwavelength techniques. This had not previously been attempted and for groups wishing to assess the spatial resolution of their sub-wavelength T-ray systems this Leeds test phantom is commercially available.

Resolution is also dependent upon the detector chosen, noise in the system, additional artifacts and so on. For example, Gafchromic film has a better resolution than OBI as the detection method of using Gafchromic film has less noise.

T-ray resolution can be improved by using various techniques such as confocal microscopy [where the spatial resolution limit reduces realistically to ~λ/2 (43)], near field imaging [resolution of ~λ/6 (33,44)] and dark field imaging. T-ray imaging technologies have been developed that are faster and can provide higher resolution than raster scanning. A flat-bed scanner is one such example (12). The Leeds test phantom utilised here would be able to determine the resolution of these systems down to 5 lp/mm (0.2 mm). T-ray imaging techniques are developing quickly. The application of these new techniques will multiply as sources and detectors develop and become more affordable.

Contrast sensitivity

Contrast is calculated as in equation (1). The contrast sensitivity was measured for X-rays with a 25×25 cm^2 field size and was found to be 33.3 [with the 13^{th} circle (see *Figure 6D*) being distinguishable with a contrast of 3%]

with settings of 65 kV, 200 mA, 16 ms. This is shown in *Figure 6C*. With a 1 mm Cu plate at settings 85 kV, 25 mA, 4 sec the contrast of the 12th disc is 2.33%, giving a contrast sensitivity of 43. Contrast differences between 2-4% are expected with a dose rate of 0.3 μGys^{-1} (45). This will vary with various voltage waveforms so the same rates are usually kept for quality assurance comparisons. Contrast sensitivity is found by the number of the last distinguishable circle.

The T-ray contrast sensitivity using the same Leeds test phantom at 0.1 THz with a 1.5 mm step size was able to distinguish all 19 discs with a contrast of 40% (giving a contrast sensitivity of 2.5). Five of these are unable to be discerned with X-rays (discs 14-18). These discs are shown clearly in a T-ray image in *Figure 6A*. A phantom more suited to T-ray contrast would be able to push past this 2.5 limit. However this shows that the phantom's contrast circle material imaged here can be better detected in this case by the T-rays, but not applied for T-ray contrast sensitivity measurement. Discs 4-7 were also imaged at 0.3 THz using 0.6 mm step sizes again on the two-colour system (Golay Cell). It was found that these discs have contrasts in the range 30-40%. These do not vary much or uniformly thus these discs have little difference in contrast using T-rays (but rather the same contrast value), as shown in *Figure 6B*.

A phantom made out of materials [perhaps different oil and water emulsions (46) or TX151 gel (47)] or a nylon step wedge developed in (23) that would give better contrast in the T-rays is needed to measure the contrast sensitivity of these T-ray systems.

Conclusions

The T-ray broadband source, with (0.1-0.4) THz penetrating the sample, was able to resolve the Leeds fluoroscopy test phantom when imaging with an aperture. This gave a spatial resolution of 0.56 lp/mm. Thus the phantom may be used for the evaluation of sub-wavelength systems or powerful systems resolution. X-rays are able to resolve the Leeds test phantom with a better resolution of 1.25 lp/mm. The same test phantom may be utilised to determine other T-ray and X-ray system's resolution. Specially made test phantoms for T-ray imaging spatial resolution determination are not necessary using sub-wavelength T-ray imaging techniques. Contrast phantoms will still need to be especially made for T-ray systems as the contrast mechanisms between T-rays and X-rays are vastly different. The contrast sensitivity of X-rays using an OBI was found to be 43 with a 1 mm copper plate at 65 kV. T-ray contrast sensitivity cannot be found using the TOR18FG as all circles gave the same contrast i.e. 40% at 0.1 THz. T-rays are better at imaging hydrated materials than X-rays; as expected. Different materials, utilising the different contrast mechanisms of T-rays, need to be used for an effective T-ray contrast phantom.

Acknowledgements

This work was supported by the Australian Research Council. The co-operation Martin Carolan and of Illawarra Cancer Care Centre in using their: Gulmay Orthovoltage unit, scanner, Leeds phantom and OBI, is very much appreciated.

Disclosure: This article has not been published elsewhere. Nor is it under submission elsewhere. This article did not meet the journal of Physics in Medicine and Biology criteria. There are no companies with interests in this work.

References

1. Humphreys K, Loughran JP, Gradziel M, et al. Medical applications of terahertz imaging: a review of current technology and potential applications in biomedical engineering. Conf Proc IEEE Eng Med Biol Soc 2004;2:1302-5.
2. Brundermann E, Heugen U, Schiwon R, et al. Terahertz imaging applications in spectroscopy of biomolecules. Microwave Symposium Digest, 2005 IEEE MTT-S International 2005.
3. Pickwell-MacPherson E, Huang S, et al. Terahertz image processing methods for biomedical applications. Conf Proc IEEE Eng Med Biol Soc 2008;2008:3751-4.
4. Duling IN, White J, Williamson S. High speed imaging with time domain terahertz. Infrared Millimeter and Terahertz Waves (IRMMW-THz), 2010 35th International Conference 2012:1.
5. Ho L, Cuppok Y, Muschert S, et al. Effects of film coating thickness and drug layer uniformity on in vitro drug release from sustained-release coated pellets: a case study using terahertz pulsed imaging. Int J Pharm 2009;382:151-9.
6. Liu HB, Zhong H, Karpowicz N, et al. Terahertz Spectroscopy and Imaging for Defense and Security Applications. Proceedings of the IEEE 2007;95:1514-27.
7. Abraham E, Younus A, Delagnes JC, et al. Terahertz-pulse imaging for non-destructive analysis of layered art paintings. Infrared Millimeter and Terahertz Waves

(IRMMW-THz), 2010 35th International Conference 2010:1-2.
8. Foulds AP, Chamberlain JM, Berry E. Terahertz imaging of wound healing. High Frequency Postgraduate Student Colloquium, 2002.7th IEEE, 2002.
9. Huang SY, Macpherson E, Zhang YT. A Feasibility Study of Burn Wound Depth Assessment Using Terahertz Pulsed Imaging. Medical Devices and Biosensors, 2007. ISSS-MDBS 2007. 4th IEEE/EMBS International Summer School and Symposium 2007:132-5.
10. Woodward RM, Wallace VP, Pye RJ, et al. Terahertz pulse imaging of ex vivo basal cell carcinoma. J Invest Dermatol 2003;120:72-8.
11. Berry E, Handley JW, Fitzgerald AJ, et al. Multispectral classification techniques for terahertz pulsed imaging: an example in histopathology. Med Eng Phys 2004;26:423-30.
12. Buzug TM, Kohl-Bareis M. Medical Imaging in the [1012Hz - 1014Hz] Domain. Annual International Conference of the IEEE Engineering in Medicine and Biology Society - EMBC, 2005.
13. Yu C, Fan S, Sun Y, et al. The potential of terahertz imaging for cancer diagnosis: A review of investigations to date. Quant Imaging Med Surg 2012;2:33-45.
14. Zhang XC. Terahertz wave imaging: horizons and hurdles. Phys Med Biol 2002;47:3667-77.
15. Chan WL, Deibel J, Mittleman DM. Imaging with terahertz radiation. Rep Prog Phys 2007;70:1325-79.
16. Du J, Hellicar AD, Li L, et al. Terahertz imaging using a high-Tc superconducting Josephson junction detector. Supercond Sci Technol 2008;21:122001-5027.
17. Zhong H, Xu J, Xie X, et al. Nondestructive defect identification with terahertz time-of-flight tomography. IEEE Sensors Journal 2005;5:203-8.
18. Brahm A, Kunz M, Riehemann S, et al. Volumetric spectral analysis of materials using terahertz-tomography techniques. Infrared Millimeter and Terahertz Waves (IRMMW-THz), 2010 35th International Conference 2010:1-2.
19. Bolduc M, Marchese L, Tremblay B, et al. Video-rate THz imaging using a microbolometer-based camera. Infrared Millimeter and Terahertz Waves (IRMMW-THz), 2010 35th International Conference 2010:1-2.
20. Jiang Z, Zhang XC. Single-shot spatiotemporal terahertz field imaging. Opt Lett 1998;23:1114-6.
21. Knab JR, Adam AJ, Nagel M, et al. Near-field THz imaging and characterization of an array of sub-wavelength circular apertures. Infrared, Millimeter and Terahertz Waves, 2008. IRMMW-THz 2008. 33rd International Conference 2008:1-2.
22. Chen HT, Kersting R, Cho GC. Terahertz imaging with nanometer resolution. Applied Physics Letters 2003;83:3009-11.
23. Fitzgerald AJ, Berry E, Miles RE, et al. Evaluation of image quality in terahertz pulsed imaging using test objects. Phys Med Biol 2002;47:3865-73.
24. Popescu DC, Hellicar AD. Point spread function estimation for a terahertz imaging system. EURASIP J Adv Signal Process 2010;2010;92.
25. Li YD, Li Q, Ding SH, et al. Resolution measurement of a 2.52 THz continuous-wave terahertz scanning imaging system. Optoelectronics and Microelectronics Technology (AISOMT), 2011 Academic International Symposium 2011:90-3.
26. Tian Z, Dudley R, Jayes L, et al. Evaluation of 3D spatial resolution for Terahertz pulsed imaging systems. Infrared and Millimeter Waves, 2007 and the 2007 15th International Conference on Terahertz Electronics. IRMMW-THz. Joint 32nd International Conference 2007:1014-5.
27. Zinovev NN, Andrianov AV, Gallant AJ, et al. Enhancement of contrast and spatial resolution in confocal coherent terahertz imaging system. Infrared Millimeter and Terahertz Waves (IRMMW-THz), 2010 35th International Conference 2010:1-2.
28. Leeds Test Objects Ltd. X-ray Test Objects Quality Assurance. Boroughbridge2006 [cited 2012 26/07/2012]; Available online: http://www.lifemed.fi/TOR18FG_esite.pdf
29. Leeds Test Objects Ltd. Test Objects. 2012 [cited 2012 26/07/2012]; Available online: http://www.e-radiography.net/radtech/l/leedstest%20object.htm
30. Pogson EM, Lewis RA, Koeberle M, et al. Terahertz time-domain spectroscopy of nematic liquid crystals. SPIE 2010;7728:77281Y1-12.
31. Loffler T, Siebert KJ, Hasegawa N, et al. All-Optoelectronic Terahertz Imaging Systems and Examples of Their Application. Proceedings of the IEEE 2007;95:1576-82.
32. Metcalfe P, Kron T, Hoban P. eds. Physics Of Radiotherapy X-Rays And Electrons. 2nd ed. USA: Medical Physics Publishing, 2007.
33. Knobloch P, Schildknecht C, Kleine-Ostmann T, et al. Medical THz imaging: an investigation of histo-pathological samples. Phys Med Biol 2002;47:3875-84.
34. Hajdok G, Battista JJ, Cunningham IA. Fundamental x-ray interaction limits in diagnostic imaging detectors: spatial resolution. Med Phys 2008;35:3180-93.

35. Henry SC, Zurk LM, Schecklman S, et al. Three-dimensional broadband terahertz synthetic aperture imaging. Optical Engineering 2012;51:091603-1.
36. Donovan EM, James H, Bonora M, et al. Second cancer incidence risk estimates using BEIR VII models for standard and complex external beam radiotherapy for early breast cancer. Med Phys 2012;39:5814-24.
37. Doi A, Blanchard F, Tanaka T, et al. Improving Spatial Resolution of Real-Time Terahertz Near-Field Microscope. J Infrared Milli Terahz Waves 2011 2011;32:1043-51.
38. Huber AJ, Keilmann F, Wittborn J, et al. Terahertz Near-Field Nanoscopy of Mobile Carriers in Single Semiconductor Nanodevices. Nano Letters 2008;8:3766-70.
39. Schuster F, Coquillat D, Videlier H, et al. Broadband terahertz imaging with highly sensitive silicon CMOS detectors. Opt Express 2011;19:7827-32.
40. Bitzer A, Ortner A, Walther M. Terahertz near-field microscopy with subwavelength spatial resolution based on photoconductive antennas. Appl Opt 2010;49:E1-6.
41. Ferguson B, Abbott D. De-noising techniques for terahertz responses of biological samples. Microelectronics Journal 2001;32:943-53.
42. Leeds Test Objects Ltd. TOR18FG User Manual. In:Leeds Test Objects Ltd, Boroughbridge, North Yorkshire 2012.
43. Fitzgerald AJ, Berry E, Zinovev NN, et al. An introduction to medical imaging with coherent terahertz frequency radiation. Phys Med Biol 2002;47:R67-84.
44. Chen Q, Jiang Z, Xu GX, et al. Near-field terahertz imaging with a dynamic aperture. Opt Lett 2000;25:1122-4.
45. Dendy PP, Heaton B. eds. Physics for Diagnostic Radiology. 2nd ed. Bristol and Philadelphia: Institute of Physics Publishing, 2003.
46. Reid C, Gibson AP, Hebden JC, et al. eds. An oil and water emulsion phantom for biomedical terahertz spectroscopy. Medical Devices and Biosensors, 2007. ISSS-MDBS 2007. 4th IEEE/EMBS International Summer School and Symposium 2007:25-4.
47. Walker GC, Berry E, Smye SW, et al. Materials for phantoms for terahertz pulsed imaging. Phys Med Biol 2004;49:N363-9.

Cite this article as: Pogson EM, McNamara J, Metcalfe P, Lewis RA. Comparing and evaluating the efficacy of the TOR18FG Leeds test X-ray phantom for T-rays. Quant Imaging Med Surg 2013;3(1):18-27. doi: 10.3978/j.issn.2223-4292.2013.02.05

